ALT 12
Advanced Laser Technologies
2 – 6 September 2012, Thun, Switzerland

ALT 12
c/o Bern University of Applied Sciences
Engineering and Information Technology
Pestalozzistrasse 20, CH-3400 Burgdorf
info@alt12.org, www.alt12.org
0041 (0) 34 426 42 06

EFFICIENT FEMTOSECOND OPTICAL PARAMETRIC AMPLIFICATION AND WAVELENGTH CONVERSION IN SILICON WAVEGUIDES

Authors:

H. Liu, Z. Wang, J. Wen, N. Huang, Q. Sun

DOI: 10.12684/alt.1.90

Corresponding author: H. Liu

e-mail: liuhongjun@opt.ac.cn

Efficient femtosecond optical parametric amplification and wavelength conversion in silicon waveguides

H. Liu*, Z. Wang, J. Wen, N. Huang, and Q. Sun

State Key Laboratory of Transient Optics and Photonics Technology, Xi'an Institute of Optics and Precision Mechanics, Chinese Academy of Science (CAS), Xi'an, 710119

*E-mail: liuhongjun@opt.ac.cn

Abstract

Efficient femtosecond optical parametric amplification and wavelength conversion via four-wave mixing (FWM) in silicon waveguides are demonstrated. In the femtosecond FWM process, the spectra are greatly broadened, and it is difficult to achieve efficient wavelength conversion and parametric amplification when the pump and signal pulse widths are close to or less than 100 fs because of the spectral overlap. The spectral overlap can be suppressed by tailoring the dispersion profiles of the silicon waveguides, and separable spectra are obtained for parametric amplification with 200 fs pulses. On-chip parametric gain as high as 26.8 dB and idler conversion gain of 25.6 dB is achieved with a low pump peak power over a flat bandwidth of 400 nm in a 10-mm-long dispersion engineered silicon waveguide. In addition, the impact of initial chirp on the wavelength conversion is also investigated, and relative narrower FWM spectra with most of the energy remain in the central peak can be obtained using appropriate initial chirp. The conversion bandwidth greater than 500 nm with peak conversion efficiency of -1.6 dB can be obtained.

Introduction

Silicon-based optical devices with micro-nano structures can offer a variety of nonlinear effects that can be used to process optical signal at the high speed of 100 Gbit/s and beyond, detect signals at unprecedented sensitivities for novel sensing applications and enable broadband electro-optic modulation. In recent years, the nonlinear silicon photonics has attracted a great deal of attention because of its potentially lower cost and high compatibility with CMOS industry, which is interested in combining new optical functionalities with electronics on a single chip. Compared with the conventional high nonlinear fibers, the silicon-on-insulator (SOI) platform has inherent advantages due to the large values of Kerr parameter and Raman gain coefficient, the flexible dispersion engineering and the tight confinement of optical mode [1]. In order to better understand the potential of silicon as a nonlinear material, various nonlinear effects have been intensively studied theoretically and experimentally [2-8]. Parametric processes via FWM have been explored in silicon waveguides typically on time scales ranged from the continuous-wave to the picosecond regime. In detail, parametric gain with a 1.8 dB gain over 60 nm bandwidth has been demonstrated in silicon waveguides with picosecond pump [6]. The conversion efficiency of -8.6 dB using reverse biased p-i-n rib waveguides was obtained with continuous-wave pump [7]. On-chip optical parametric oscillator based on the silicon waveguide can generate more than 100 new wavelengths with operating powers below 50 mW [8]. Despite these progresses, there is still a strong motivation to explore femtosecond optical parametric amplification and wavelength conversion in silicon waveguides.

Here, we demonstrate efficient femtosecond parametric amplification and wavelength conversion via degenerate FWM in silicon rib waveguides. The influences of spectral broadening, dispersion profiles and initial chirp on the parametric process are investigated. The on-chip parametric gain as high as 26.8 dB and broad bandwidth more than 400 nm are obtained for a pump peak power of 10 W in a dispersion engineered silicon rib waveguide. After optimizing the initial chirp of the pump and signal pulses, ultrabroadband wavelength conversion in the silicon rib waveguide is achieved with bandwidth of over 500 nm and peak conversion efficiency of -1.6 dB.

Theory

Here, we focus on the degenerate FWM, which typically involves two pump photons at frequency ω_p transporting their energy to a signal wave at frequency ω_s and an idler wave at frequency ω_i as the relation $2\omega_p=\omega_s+\omega_i$ holds. The pump, signal and idler waves are identically polarized in the fundamental quasi-TE mode. To describe the nonlinear optical interaction of the pump, signal and idler in the waveguide, we use the formulism described in [9] and take into account the effects of two-photon absorption (TPA), free-carrier absorption (FCA), and free-carrier dispersion (FCD). Remarkably, the stimulated Raman scattering (SRS) is negligible for femtosecond pulses propagating in silicon waveguides because

the Raman response time is about 3 ps and SRS is only effective for pulses longer than this [10]. The equations that govern the evolution of the different waves read as:

$$\begin{aligned}&\frac{\partial A_p}{\partial z}+\frac{i\beta_{2p}}{2}\frac{\partial^2 A_p}{\partial T^2}-\frac{\beta_{3p}}{6}\frac{\partial^3 A_p}{\partial T^3}\\&=-\frac{1}{2}\left(\alpha_p+\alpha_{fcp}\right)A_p+i\gamma_{pe}\left(1+\frac{i}{\omega_p}\frac{\partial}{\partial T}\right)\left|A_p\right|^2 A_p\\&\quad+i\frac{2\pi}{\lambda_p}\delta_{nfcp}A_p+2i\gamma_{pe}\left(\left|A_s\right|^2+\left|A_i\right|^2\right)A_p\\&\quad+2i\gamma_p A_s A_i A_p^{*}\exp\left(i\Delta\beta z\right),\end{aligned}\tag{1}$$

$$\begin{aligned}&\frac{\partial A_s}{\partial z}+d_s\frac{\partial A_s}{\partial T}+\frac{i\beta_{2s}}{2}\frac{\partial^2 A_s}{\partial T^2}-\frac{\beta_{3s}}{6}\frac{\partial^3 A_s}{\partial T^3}\\&=-\frac{1}{2}\left(\alpha_s+\alpha_{fcs}\right)A_s+i\gamma_{se}\left(1+\frac{i}{\omega_s}\frac{\partial}{\partial T}\right)\left|A_s\right|^2 A_s\\&\quad+i\frac{2\pi}{\lambda_s}\delta_{nfcs}A_s+2i\gamma_{se}\left(\left|A_p\right|^2+\left|A_i\right|^2\right)A_s\\&\quad+i\gamma_s A_p^2 A_i^{*}\exp\left(-i\Delta\beta z\right),\end{aligned}\tag{2}$$

$$\begin{aligned}&\frac{\partial A_i}{\partial z}+d_i\frac{\partial A_i}{\partial T}+\frac{i\beta_{2i}}{2}\frac{\partial^2 A_i}{\partial T^2}-\frac{\beta_{3i}}{6}\frac{\partial^3 A_i}{\partial T^3}\\&=-\frac{1}{2}\left(\alpha_i+\alpha_{fci}\right)A_i+i\gamma_{ie}\left[1+\frac{i}{\omega_i}\frac{\partial}{\partial T}\right]\left|A_i\right|^2 A_i\\&\quad+i\frac{2\pi}{\lambda_i}\delta_{nfci}A_i+2i\gamma_{ie}\left(\left|A_p\right|^2+\left|A_s\right|^2\right)A_i\\&\quad+i\gamma_i A_p^2 A_s^{*}\exp\left(-i\Delta\beta z\right),\end{aligned}\tag{3}$$

where A_j is the slowly varying amplitude (j=p, s, i), z is the propagation distance, β_{2j} is the group-velocity dispersion (GVD) coefficient and β_{3j} is the third-order dispersion (TOD) coefficient. $T=t-z/v_{gp}$ is measured in a reference frame moving with pump pulse traveling at speed v_{gp}. The two walk-off parameters of the signal and idler are defined as $d_s=\beta_{1s}-\beta_{1p}$ and $d_i=\beta_{1i}-\beta_{1p}$, respectively, where β_{1j} is the inverse of the group velocity. The nonlinear coefficient γ_{je} is given by [11]

$$\gamma_{je}=\gamma_j+i\frac{\beta_{\mathrm{TPA}}}{2A_{eff}},\tag{4}$$

where $\gamma_j=\omega_j n_2/cA_{eff}$ is the effective nonlinearity of the waveguide, $n_2=12\pi^2\chi^{(3)}/n_0 c$ is the nonlinear index coefficient, c is the speed of light in vacuum, n_0 is the linear refractive index, A_{eff} is the effective area of the propagating mode and β_{TPA} is the coefficient of TPA. Here $n_2=6\times10^{-18}$ m^2W^{-1} and $\beta_{TPA}=5\times10^{-12}$ mW^{-1} in the 1550-nm regime [4].

In Eqs. (1)-(3), α_j accounts for the linear loss and $\alpha_{fcj}=\sigma_j N_c$ represents FCA, where σ_j is the free carrier absorption cross section and N_c is the free-carrier density. The free-carrier induced index change is $\delta_{nfcj}=\zeta_j N_c$. These free-carrier parameters can be obtained by the following equations [11]

$$\sigma_j=1.45\times10^{-21}\left(\lambda_j/\lambda_{ref}\right)^2\ \mathrm{m}^2,\tag{5}$$

$$\zeta_j=-1.35\times10^{-27}\left(\lambda_j/\lambda_{ref}\right)^2\ \mathrm{m}^3,\tag{6}$$

$$\frac{\partial N_c(z,t)}{\partial t}=\frac{\pi\beta_{TPA}}{h\omega_p A_{eff}^2}\left|A_p(z,t)\right|^4-\frac{N_c(z,t)}{\tau_c},\tag{7}$$

where λ_j is the wavelength, λ_{ref}=1550 nm, h is Planck's constant, and the carrier lifetime is $\tau_c\approx1$ ns. Here, free carriers induced by the signal and idler are negligible compared with that induced by the pump in the parametric amplification process.

The parametric process is numerically studied by simultaneously injecting pump pulses and signal pulses with same pulse width and same repetition rate in silicon rib waveguides. The rib height (H) and the etch depth (h) are 300 nm and 260 nm, respectively. In general, the quasi-phase-matching can be satisfied if the pump wavelength is located in the anomalous GVD regime [6, 11]. Careful choice of the waveguide width (W) is required to obtain anomalous-GVD at the pump center wavelength (1550 nm) and we can change the rib waveguide width to tailor the zero-dispersion wavelength (ZDWL). The widths satisfied the anomalous-GVD condition at the pump wavelength must be a range, and we choose 550 nm, 600 nm and 650 nm from the series of widths as the waveguide widths. The GVD of the three waveguides is shown in Fig. 1. The effective mode areas A_{eff} are 0.09 μm^2, 0.12 μm^2 and 0.15 μm^2 for the above-mentioned waveguides, respectively. The linear propagation losses of the three waveguides are assumed to be 0.3 dB/cm, 0.25 dB/cm and 0.22 dB/cm, respectively [12].

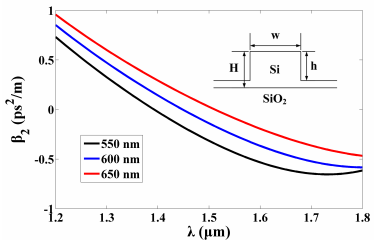

Fig. 1. Schematic diagram of rib silicon waveguide and GVD for different waveguide widths

Results

Figure 2 depicts the spectra at the input and output of the rib waveguide with 550 nm width for a 1550 nm pump with 5 W peak power and 1450 nm signal with 1 W peak power when the pump and signal pulse width are 100 fs, 300 fs, and 500 fs, respectively. It is clear that the signal was efficiently converted and amplified into an idler at wavelength of 1665 nm. Because of self-phase modulation (SPM) and cross-phase modulation (XPM) in the FWM process, all of the output spectra are broadened and spectral overlap appears for the 100 fs pulses as shown in Fig. 2. It is found that the spectral broadening is much larger for shorter pulses in the femtosecond regime and spectral overlap can not avoid in this case for pulses,

which are less than 100 fs. Therefore it is difficult to achieve a wavelength converter and amplifier when the input pump and signal pulse widths are close to or less than 100 fs because it is difficult to separate the signal and idler from the pump.

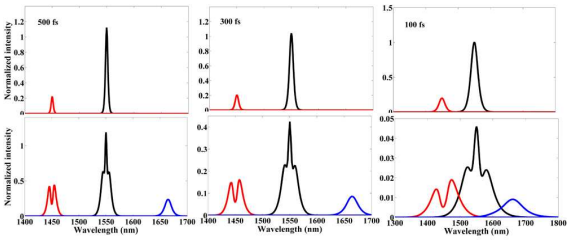

Fig. 2. The input and output spectrum in the 1.5-mm-long silicon rib waveguide for different pulse widths, respectively.

We simulate the OPA process using 200 fs pump and signal pulses. The lengths of the three waveguides are 10 mm and the input pump peak power is 5 W, while the signal peak power is 1 mW. The repetition rate of pump and signal pulses is 0.1 GHz, which means low free carrier effects for femtosecond pulses. Figure 3 shows the spectra of the pump, signal and idler from the three waveguides. The spectrum of the pump is greatly broadened when the width of the waveguide is 550 nm, covering the signal and idler spectra as shown in Fig. 3 (a). With increasing the width of the waveguide, the degree of spectral broadening is decreasing. Fig. 3 (c) shows the signal and idler spectra only have little overlap with the pump spectrum. Therefore, separable spectra can be achieved by tailoring the dispersion profiles of the silicon waveguide.

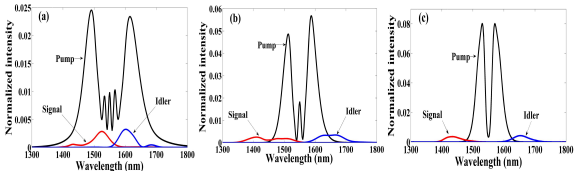

Fig. 3. Output spectra of the waveguides with widths of (a) 550 nm, (b) 600 nm and (c) 650 nm.

The relationship between the on-chip parametric gain and signal center wavelength is depicted in Fig. 4(a) for a pump peak power of 10 W. The gain curves are symmetric around pump wavelength, so only the halves of them are plotted. The signal center wavelengths that vary from 1350 nm to 1450 nm are considered in the following simulations for longer wavelengths that ranging from 1460 nm to 1540 nm will result in spectra overlap. Here, we define the on-chip parametric signal gain (idler conversion gain) as the ratio of the output pulse energy of the signal (idler) to the input signal pulse energy, such that: $G_s=10log_{10}(E_{sout}/E_{sin})$, $G_s=10log_{10}(E_{iout}/E_{sin})$. From Fig. 4(a), one can find that a broad bandwidth of the femtosecond OPA can be obtained in the silicon rib waveguide with well gain flatness. As can be seen from Fig. 4(a), when the signal wavelength is 1450 nm, the maximum signal and idler on-chip gains reach 26.8 dB and 25.6 dB, respectively. When the signal wavelength is 1350 nm, the minimal gains are 21.8 dB and 20.5 dB, respectively. It is clear that the on-chip gain is large enough to overcome the fiber-chip coupling losses that are about 13 dB. Considering the whole gain curve, the FWM bandwidth is larger than 400 nm for a pump peak power of 10 W.

The on-chip parametric signal gain and idler conversion gain versus pump peak power are shown in Fig. 4 (b) for signal wavelength of 1400 nm. It is found that the gains become larger as the pump power increases, and gain saturation appears when the pump peak power exceeds 6 W due to the increasing nonlinear losses and phase mismatch as the pump peak power increases. Remarkably, FCA plays a significant role for a high repetition rate (>1 GHz). In this case, the on-chip gain will decrease, and when repetition rate reach 100 GHz the gain may even to be zero. One way to overcome the obstacle for high repetition rate OPA is to use a reverse-biased p-i-n diode structure to reduce the carrier lifetime.

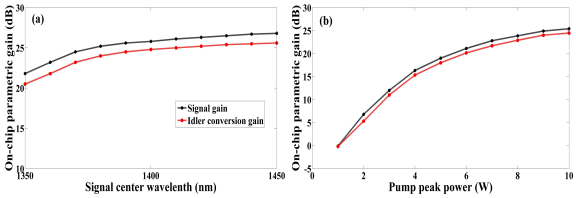

Fig. 4. On-chip parametric gain as a function of (a) signal center wavelength and (b) pump peak power.

The above FWM process are simulated with unchirped pulses. However, the initial chirp can lead to drastic changes in the pulse spectrum. Figure 5 shows the spectra at the output of the rib waveguide with width of 650 nm for a 1550 nm pump and 1450 nm signal with different initial chirps. Both of the pulse width of the input pump and signal are 200 fs with peak power of 6 W and 1 W, respectively. Separable FWM spectra with most of the energy remains in the central peak can be obtained by optimizing the initial chirp. In this case, the optimal chirp is a range from -1 to -2 as shown in Fig. 5.

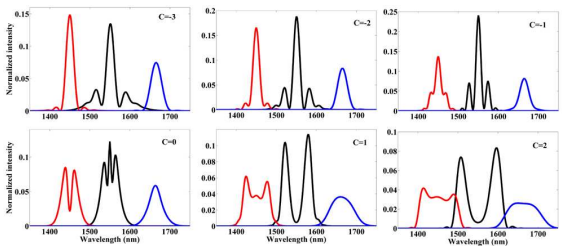

Fig. 5. The output spectra in the 3.2-mm-long silicon rib waveguide for a 1550 nm pump and a 1450 nm signal with different initial chirps.

Figure 6(a) shows the FWM spectra with signal tuned from 1350 to 1500 nm. The repetition rate of pump and signal pulses is 40 GHz with initial chirp C=-2. Therefore, efficient wavelength conversion can be achieved using this rib waveguide with flat bandwidth over 500 nm. The conversion efficiency as a function of signal wavelength is shown in Fig. 6(b), and conversion efficiency as high as -1.6 dB is obtained.

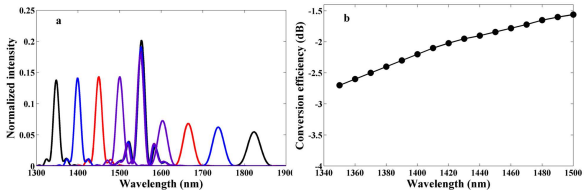

Fig. 6. (a) The output spectra in the 3.2-mm-long silicon waveguide for signal centered at 1350, 1400, 1450, and 1500 nm, respectively. (b) Conversion efficiency as a function of signal wavelength.

Conclusion

We demonstrate efficient femtosecond parametric amplification and wavelength conversion via degenerate FWM in silicon rib waveguides. The influences of spectral broadening, dispersion profiles and initial chirp on the parametric process are investigated. First, it is difficult to achieve efficient wavelength conversion and parametric amplification when the pump and signal pulse widths are close to or less than 100 fs because of the spectral overlap. Moreover, the spectral overlap can be suppressed by tailoring the dispersion profiles of the silicon waveguides, and separable spectra are obtained for parametric amplification with 200 fs pulses. The on-chip parametric gain as high as 26.8 dB over a flat bandwidth of 400 nm are obtained for a pump peak power of 10 W in a dispersion engineered silicon rib waveguide. After optimizing the initial chirp of the pump and signal pulses, relative narrower FWM spectra with most of the energy remain in the central peak can be obtained. Ultrabroadband wavelength conversion in the silicon rib waveguide is achieved with bandwidth over 500 nm and peak conversion efficiency of -1.6 dB.

References

[1] J. Leuthold, C. Koos and W. Freude (2010), Nonlinear silicon photonics, Nature Photonics, 4, 535-544.

[2] H. Rong, R. Jones, A. Liu, O. Cohen, D. Hak, A. Fang and M. Paniccia (2005), A Continuous-wave Raman silicon laser, Nature, 433, 725-728.

[3] Y. Liu and H. K.Tsang (2007), Time dependent density of free carriers generated by two photon absorption in silicon waveguides, Appl. Phys. Lett., 90, 211105.

[4] L. Yin and G. P. Agrawal (2007), Impact of two-photon absorption on self-phase modulation in silicon waveguides, Opt. Lett., 32, 2031-2033.

[5] I.-W. Hsieh, X. Chen, J. I. Dadap, N. C. Panoiu and R. M. Osgood Jr. (2007), Cross-phase modulation-induced spectral and temporal effects on co-propagating femtosecond pulses in silicon photonic wires, Opt. Express, 15, 1135-1146.

[6] M. A. Foster, A. C. Turner, J. E. Sharping, B. S. Schmidt, M. Lipson and A. L. Gaeta (2006), Broad-band optical parametric gain on a silicon photonic chirp, Nature, 441, 960-963.

[7] Y. H. Kuo, H. Rong, V. Sih, S. Xu, M. Paniccia and O. Cohen (2006), Demonstration of wavelength conversion at 40 Gb/s data rate in silicon waveguides, Opt. Express, 14, 11721-11726.

[8] J. S. Levy, A. Gondarenko, M. A. Foster, A. C. Turner-Foster, A. L. Gaeta and M. Lipson (2010), CMOS-compatible multiple-wavelength oscillator for on-chip optical interconnects, Nature Photonics, 4, 37-40.

[9] G. P. Agrawal (2007), Nonlinear Fiber Optics, Academic Press.

[10] Q. Lin, O. J. Painter and G. P. Agrawal (2007), Nonlinear optical phenomena in silicon waveguides: Modeling and applications, Opt. Express, 15, 16604-16644.

[11] Q. Lin, J. Zhang, P. M. Fauchet and G. P. Agrawal (2006), Ultrabroadband parametric generation and wavelength conversion in silicon waveguides, Opt. Express, 14, 4786-4799.

[12] W. Mathlouthi, H. Rong and M. Paniccia (2008), Characterization of efficient wavelength conversion by four-wave mixing in sub-micron silicon waveguides, Opt. Express, 16, 16735-16745.

Acknowledgments

This work was supported by the National Natural Science Foundation of China under Grant 61078029 and 61178023.